Parameter estimation for whole-body kinetic model of FDG metabolism*

CUI Yunfeng[1], BAI Jing[1]**, CHEN Yingmao[2] and TIAN Jiahe[2]

(1. Department of Biomedical Engineering, Tsinghua University, Beijing 100084, China; 2. Department of Nuclear Medicine, General Hospital of PLA, Beijing 100853, China)

Received January 13, 2006; revised April 21, 2006

Abstract Based on the radioactive tracer [^{18}F] 2-fluoro-2-deoxy-D-glucose (FDG), positron emission tomography (PET), and compartment model, the tracer kinetic study has become an important method to investigate the glucose metabolic kinetics in human body. In this work, the kinetic parameters of three-compartment and four-parameter model for the FDG metabolism in the tissues of myocardium, lung, liver, stomach, spleen, pancreas, and marrow were estimated through some dynamic FDG-PET experiments. Together with published brain and skeletal muscle parameters, a relatively complete whole-body model was presented. In the liver model, the dual blood supply from the hepatic artery and the portal vein to the liver was considered for parameter estimation, and the more accurate results were obtained using the dual-input rather than the single arterial-input. The established whole-body model provides the functional information of FDG metabolism in human body. It can be used to further investigate the glucose metabolism, and also be used for the simulation and visualization of FDG metabolic process in human body.

Keywords: compartment model, FDG, PET, parameter estimation.

The anatomical and functional information about human body are beneficial to human being's health care and disease diagnosis and treatment. How to comprehensively understand and efficiently use this information have become more and more important in many research fields and industry. For example, the Visible Human Project (VHP) provides a set of detailed anatomical information of human body and has been widely used in the medical imaging segmentation, reconstruction, and 3D visualization[1—4]. The research on human anatomy has been developed very well and more attentions were paid to the functional information in recent years.

The functional information of glucose metabolism is one of the most important functional information in human body. With the development of positron emission tomography (PET) technology, the tracer kinetic study has become a main method to investigate the glucose metabolism such as the local glucose metabolic rate in human body[5—7]. [^{18}F] 2-fluoro-2-deoxy-D-glucose (FDG) is one of the most common tracers for this kinetic study and it is widely used in the clinical PET experiments for malignant tumour detection. FDG has similar property to the glucose in the initial two steps of the metabolic process. The concentration of radioisotope ^{18}F included in FDG can be detected by PET instrument. In many tissues of human body, such as gray matter, white matter, myocardium, and skeletal muscle, the three-compartment and four-parameter model is used for the kinetic study of FDG and glucose metabolism and has been proved valid[5—10]. The kinetic modeling provides the functional information of FDG metabolism and it can be used as a tool to acquire more information.

However, most studies on kinetic modeling of brain, including gray matter and white matter, myocardium, or skeletal muscle investigated only one individual tissue's model for FDG metabolism and did not attempt to synthesize these individual models into a unified kinetic model. Hays et al.[11] proposed a whole-body model which includes brain, myocardium, liver, and lung. In this model, all individual tissue's models are connected with each other through their common compartment - blood compartment, making this whole-body model have a radial form. However, as mentioned in their paper, the whole-body model included only 24% of FDG metabolism in human body because many other tissues which are active in metabolism of FDG were not involved in this model. In addition, Hays et al. directly used the ar-

* Supported by National Natural Science Foundation of China (Grant No. 60331010)

** To whom correspondence should be addressed. E-mail: deabj@tsinghua.edu.cn

terial blood curve as the model input function in the liver study, but the use of arterial-input may cause systematic errors in the estimated model parameters because of the ignorance of the hepatic dual blood supply from the hepatic artery and the portal vein to the liver[12,13]. Therefore, the whole-body kinetic model of FDG metabolism may be improved in its extent and accuracy.

In this study, some dynamic FDG-PET experiments were performed and the model parameters of myocardium, lung, liver, stomach, spleen, pancreas, and marrow were estimated using the PET image data. With the parameter estimation results and the published brain and skeletal muscle parameters, a relatively complete whole-body kinetic model of FDG metabolism in human body was presented in this study. In the liver model, the dual blood supply was considered for the parameter estimation, and the more accurate results were obtained using the dual-input rather than the single arterial-input.

1 Method

1.1 Data acquisition

Five normal adult volunteers (three men, two women) were the participants in this study and the data were derived from their dynamic FDG-PET experiments. Volunteers were informed fully about the purposes and procedures of the study and gave written consent. Volunteers had emptied the bladder before the beginning of the experiment, and held themselves lying and motionless during the PET imaging. The imaging was performed using ECAT-EXACT HR+ PET scanner (CTI/Siemens, Inc., TN, USA), with a 15.5 cm field of view, 63 transaxial image planes, and a 4.2 mm full-width-at-half-maximum spatial resolution in the center field of view. The study was performed in a single bed position covering from upper heart to lower liver. This area included the target tissues myocardium, lung, liver, stomach, spleen, pancreas, and marrow. 4.10 ± 0.14 mCi of FDG was injected intravenously into the human body, and PET imaging began immediately when the injection was begun. The sampling protocol is six 10 s, eight 20 s, six 30 s, five 60 s, four 300 s, and three 600 s scans, totaling 32 frames for a total scan time of 61 minutes and 40 seconds.

1.2 PET image analysis

In order to apply the kinetic model to the PET data, it is generally necessary to obtain arterial blood time-activity curve (BTAC) and tissue time-activity curve (TTAC) from dynamic PET image data. The arterial BTAC and the TTAC are used as the input and output functions of the kinetic model respectively to estimate the model parameters. TTAC was derived by drawing a region of interest (ROI) on the target tissue in one frame which best showed the tissue. The radioactivity value of the tissue was calculated by averaging whole voxel's values within the ROI, so the large ROI can effectively suppress the effects of random noise. In this study, the ROIs was drawn as largely as possible in each plan of the 3D image data as long as the target tissue could be clearly identified in that plan. However, the edge of the figure of tissues identified in the PET images must be excluded from ROI because these regions are highly affected by spillover effects and organ motion. After drawing a ROI from one frame of a dynamic PET data, this ROI was applied to the whole frames of this dynamic PET image data, so the complete time-activity curve (TAC) was obtained. Concerning the acquisition of BTAC, although the arterial blood sampling measurements are considered to be the most accurate method, it is generally accepted that the insertion of arterial lines and the subsequent collection and processing of arterial blood are not compatible with the practice of clinical PET[14]. This method is invasive to the subject and exposes the personnel to the risks associated with the handling of blood and radiation dose[8,15]. Therefore, in this study, the arterial BTAC was evaluated using the image-derived method[16,17]. This method is similar to that of TTAC acquisition, and the ROI is drawn on left ventricle or aorta. To reduce the scattering effect of radioactivity from the adjacent tissue, in this study, the arterial BTAC was derived from aorta instead of left ventricle.

Fig. 1(a) and (b) are the same coronal section of a dynamical PET data, but the two are in different frames. Fig. 1(a) is at the time of the 35th second after FDG injection, and Fig. 1(b) is at the 57th minute. The brighter color indicates the higher concentration of radioisotope in the region. The aorta can be easily identified in Fig. 1(a) to acquire the arterial BTAC. The myocardium and liver can be easily identified in Fig. 1(b), and the other target tissues of lung, stomach, spleen, pancreas, and marrow can also be identified respectively in the other coronal, sagittal, or transaxial sections. Besides the arterial BTAC and the respective TTACs, the portal vein

BTAC was needed to consider the dual blood supply in liver tissue. Because of the low resolution of PET image, the shape of the portal vein in the PET image is not very clear. Nevertheless, it was also distinguished in the images by the experienced doctors of the department of nuclear medicine. The part marked by yellow dashed ellipse in Fig. 1(a) was identified as portal vein. To validate its position, Fig. 1(a) was recolored using pure red colormap (Fig. 1(c)), and the two images Fig. 1(b) and (c) were fused (Fig. 1(d)). It can be seen from the fused image Fig. 1(d) that the position of this portal vein in the liver is reasonable. Therefore, the portal vein BTAC was also obtained using image-derived method.

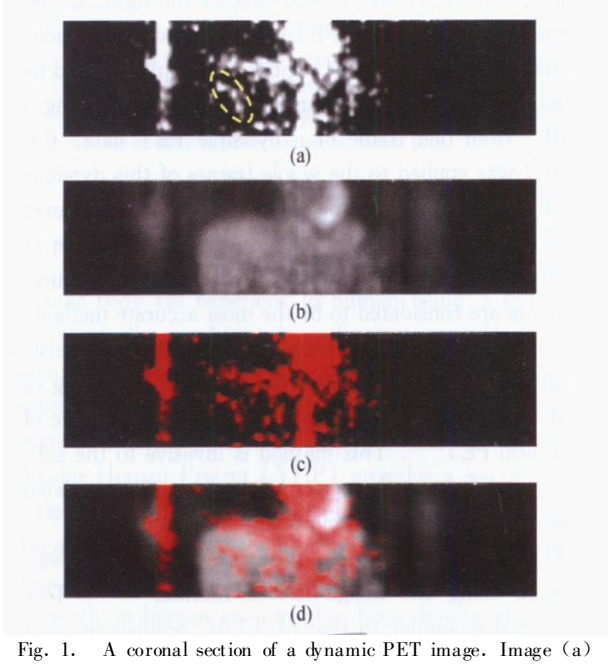

Fig. 1. A coronal section of a dynamic PET image. Image (a) and (c) are in the frame of the sampling time of the 35th second after FDG injection and shown with gray and pure red colormaps, respectively. The brighter color indicates the higher concentration of radioisotope. Image (b) is in the frame of the sampling time of the 57th minute. Image (d) is derived by fusing the images (b) and (c).

1.3 Compartment model for the individual tissue

Many tissues in human body such as gray matter, white matter, myocardium, and skeletal muscle can be described by three-compartment and four-parameter model illustrated in Fig. 2 for the FDG metabolism[5—10]. In this study, this classic model was also used to describe the FDG metabolic process in the tissues of lung, liver, stomach, spleen, pancreas, and marrow. In this model, the left compartment represents vascular space for FDG, the center compartment represents tissue space for free FDG and the right compartment represents tissue space for FDG-6-phosphate (FDG-6-P). FDG is transported across the cell membrane into the tissue cell and phosphorylated intracellularly by the enzyme hexokinase to FDG-6-phosphate (FDG-6-P). The reverse processes of these two steps are also presented in the model. The concentrations of FDG or FDG-6-P in the three compartments are C_B, C_E, and C_M, respectively. $C_B(t)$ is the ^{18}F concentration in the blood as a function of time, and it is equivalent to the BTAC because the radioactivity of ^{18}F can be easily converted into its concentration. The model parameters k_1—k_4 are the rate constants of material exchange between compartments. The spillover fraction f from blood to the tissue is also considered to be a parameter of the model. If $C_T(t)=C_i(t)+f\cdot C_B(t)$, where $C_i(t)=C_E(t)+C_M(t)$, then $C_T(t)$ is equivalent to the observed total TTAC in PET image. From this model, the following equation is obtained

$$C_T(t)=\frac{k_1}{\alpha_2-\alpha_1}((k_3+k_4-\alpha_1)e^{-\alpha_1 t}+(\alpha_2-k_3-k_4)e^{-\alpha_2 t})\otimes C_B(t)+f\cdot C_B(t), \quad (1)$$

where $\otimes$ denotes the operation of convolution, and

$$\alpha_1=(k_2+k_3+k_4-\sqrt{(k_2+k_3+k_4)^2-4k_2k_4})/2, \quad (2)$$

$$\alpha_2=(k_2+k_3+k_4+\sqrt{(k_2+k_3+k_4)^2-4k_2k_4})/2. \quad (3)$$

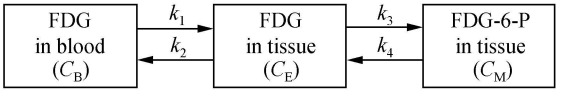

Fig. 2. The three-compartment and four-parameter model for FDG metabolism.

Thus, if $C_B(t)$ and $C_T(t)$ are given, the five model parameters k_1—k_4 and f can be calculated from Eq. (1) using curve fitting. In this parameter estimation, $C_B(t)$ is used as an input function, and it is equivalent to BTAC. $C_T(t)$ is used as output function, and it is equivalent to TTAC. The BTAC and TTAC could be obtained from dynamic PET image data by drawing appropriate ROIs.

1.4 The dual-input function for liver kinetic model

The liver has a dual blood supply from the hepatic artery and the portal vein to the liver. The single arterial-input may be not consistent with the actual model input in the liver model, and the use of arteri-

al-input may introduce errors in the estimated model parameters[12, 13]. Therefore, a dual-input function, which is generated by calculating weighted sum of both the arterial and the portal vein input curve, is needed for the liver study. According to the two blood vessels' approximate percentage perfusion to the nontumor liver tissue, in this study, the dual-input function was measured by using fixed weights from these two blood supply inputs, i.e. 20% contribution from artery and 80% contribution from portal vein[12, 13, 18]. Thus, the blood input function $C_B(t)$ in the liver model was calculated according to

$$C_B(t) = C_a(t) \times 20\% + C_v(t) \times 80\%, \quad (4)$$

where $C_a(t)$ is the arterial BTAC and $C_v(t)$ is the portal vein BTAC. In this study, the result of model parameter estimation using dual-input function was compared with that using arterial-input function.

1.5 Parameter estimation and statistical analysis

With the measurements of both BTAC and TTAC, the model parameters k_1-k_4 and f were estimated by the weighted nonlinear least square (WNLS) method. In this curve fitting, all of the individual parameters were evaluated by minimizing the weighted residual sum of squares (WRSS), which is a direct measurement of the fitting quality. WRSS is given by

$$\mathrm{WRSS}(p) = \sum_{k=1}^{32} w_k [C_T(t_k, p) - Z(t_k)]^2, \quad (5)$$

where p is the vector of parameters to be estimated, w_k is the weight adopted, which is proportional to the frame duration and inversely proportional to the radioactivity at that time point, $C_T(t)$ is the model output, which is a function of p, and Z is the tissue activity measured from PET image. The superscript 32 is the total sampling points of dynamic PET in this study.

After parameter estimation, the forward clearance K was calculated by using the following formula:

$$K = \frac{k_1 k_3}{k_2 + k_3}. \quad (6)$$

The forward clearance K can be used to determine the local metabolic rate of glucose[6].

The Akaike Information Criteria (AIC)[19] and Schwarz Criteria (SC)[20] were used to measure the quality of model fitting:

$$\mathrm{AIC} = N\ln(\mathrm{WRSS}) + 2P, \quad (7)$$

$$\mathrm{SC} = N\ln(\mathrm{WRSS}) + P\ln(N), \quad (8)$$

where P is the number of parameters in the model, and N is the number of data points.

The mean and standard deviation (SD) were calculated for each set of values, and the results were given as the mean±SD.

1.6 Whole-body model

In all individual tissue's models, the circulatory system is a common part as the model input. Thus, these individual models can be connected by circulatory system forming a distributed whole-body model. This whole-body model is illustrated in Fig. 3. In addition to the tissues investigated in this study, the brain tissues, including gray matter and white matter, and skeletal muscle were incorporated into this model, making the whole-body model more complete. The kinetic models of gray matter, white matter, and skeletal muscle were investigated by many studies and their model parameters can be derived from Ref. [6, 7, 9, 21].

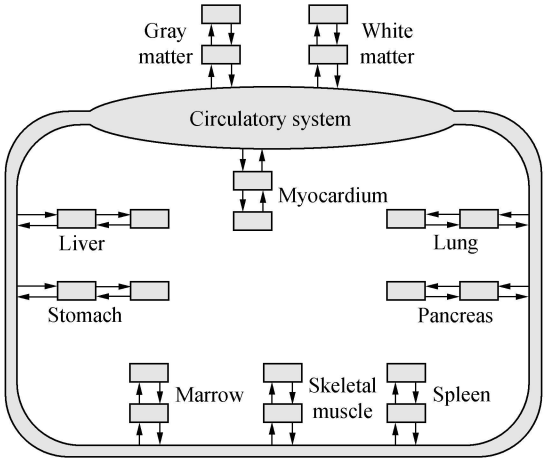

Fig. 3. Whole-body model.

2 Results

Fig. 4 shows the arterial BTAC and portal vein BTAC acquired from a dynamic PET data by drawing ROI. To observe the relation between the two curves more clearly, the two curves shown in Fig. 4 were smoothed before. The first 15 minutes are shown in this figure because the two curves are almost identical in the later times. As illustrated in Fig. 4, the peak of the portal vein BTAC is delayed and dispersed when compared with that of the arterial curve.

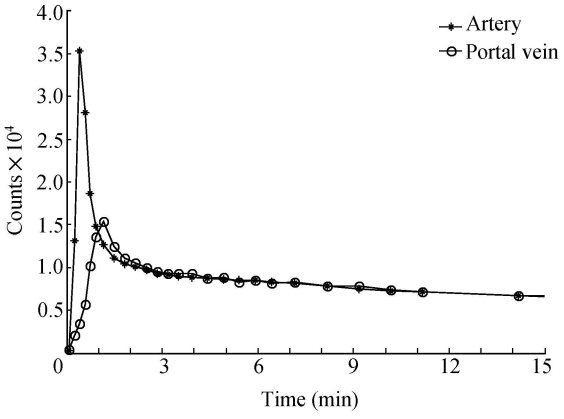

Fig. 4. The arterial BTAC and portal vein BTAC acquired from a dynamic PET image data. The first 15 min are shown, when differences of shapes of the two curves are most pronounced.

The estimated model parameters for the seven tissues and calculated values of forward clearance K and AIC and SC are shown in Table 1. The results are given as the mean±SD. In the lung model, the estimated value of k_4 was zero, indicating that the three-compartment and three-parameter model (including four parameters of k_1, k_2, k_3 and f) is more adequate to describe the FDG metabolism in lung. The program used in our work can automatically apply the three-compartment and three-parameter model to the curve fitting when the k_4 converges to zero in the iterative procedure of the nonlinear least square algorithm. The parameter estimation procedure of three-compartment and three-parameter model is similar to that of the three-compartment and four-parameter model, but the fitting algorithm for the three-compartment and three-parameter model is less affected by the initial value of parameters and converges better to a solution because of a less number of parameters to be estimated in this model.

Table 1. The results of parameter estimations, forward clearance K, and criterions in the seven tissues. (mean±SD; the number of subjects is five)

Tissue	Rate constants					$K=\frac{k_1k_3}{k_2+k_3}$	Criterion	
	$k_1(\mathrm{min}^{-1})$	$k_2(\mathrm{min}^{-1})$	$k_3(\mathrm{min}^{-1})$	$k_4(\mathrm{min}^{-1})$	f		AIC	SC
Myocardium	0.196±0.115	1.022±0.504	0.149±0.115	0.010±0.011	0.545±0.099	0.023±0.018	227.2±16.3	234.2±16.0
Lung	0.014±0.009	0.291±0.158	0.006±0.006	0.000±0.000	0.151±0.025	0.0003±0.0004	218.5±5.9	224.3±5.9
Liver	1.256±0.160	1.329±0.266	0.002±0.001	0.002±0.004	0.165±0.066	0.002±0.001	227.5±17.5	234.8±17.5
Stomach	0.614±0.218	1.885±0.538	0.071±0.023	0.031±0.009	0.063±0.023	0.021±0.006	221.8±15.1	229.1±15.1
Spleen	1.207±0.498	1.909±0.471	0.008±0.006	0.014±0.011	0.000±0.000	0.005±0.003	209.3±8.6	216.6±8.6
Pancreas	0.648±0.365	1.640±0.873	0.027±0.024	0.016±0.015	0.107±0.121	0.010±0.008	242.9±18.2	249.6±19.0
Marrow	0.425±0.179	1.055±0.427	0.023±0.006	0.013±0.005	0.040±0.025	0.009±0.002	215.3±14.9	222.6±14.9

For the liver model, the kinetic parameters were estimated using dual-input and arterial-input. The results using these two input functions were compared with each other to confirm that the dual-input analysis is necessary to the liver study. The results of parameter estimations, forward clearance K, and criterions using arterial-input and dual-input are summarized in Table 2. As seen in this table, the estimated values of k_1, k_2, and f are obviously larger using the dual-input rather than a single arterial-input. The k_3 and k_4 values do not differ significantly using either of the inputs. The values of K using the two methods are quite close to each other. AIC and SC using the dual-input are lower than those using the arterial-input, suggesting that the use of the dual-input function, instead of the conventional arterial-input function, improves model fitting and makes results more accurate.

Table 2. The results of parameter estimations, forward clearance K, and criterions using arterial-input and dual-input. (mean±SD; the number of subjects is five)

Input	Rate constants					$K=\frac{k_1k_3}{k_2+k_3}$	Criterion	
	$k_1(\mathrm{min}^{-1})$	$k_2(\mathrm{min}^{-1})$	$k_3(\mathrm{min}^{-1})$	$k_4(\mathrm{min}^{-1})$	f		AIC	SC
Arterial	0.634±0.134	0.581±0.141	0.002±0.001	0.003±0.005	0.000±0.000	0.002±0.002	252.5±12.8	259.5±12.8
Dual	1.256±0.160	1.329±0.266	0.002±0.001	0.002±0.004	0.165±0.066	0.002±0.001	227.5±17.5	234.8±17.5

3 Discussion

To validate the parameter estimation procedure performed in this study, our results of kinetic parameters of myocardium model were compared with the results given by Bertoldo et al.[21] (where $k_1=0.341\pm0.220$, $k_2=1.429\pm0.784$, $k_3=0.125\pm0.041$, $k_4=0.003\pm0.003$, $f=0.252\pm0.102$), Li et

al.[22] (where $k_4 = 0.007 \pm 0.004$, $f = 0.426 \pm 0.172$) and Li et al.[23] (where $k_1 = 0.406 \pm 0.207$, $k_2 = 1.185 \pm 0.814$, $k_3 = 0.216 \pm 0.134$, $k_4 = 0.011 \pm 0.008$, $f = 0.361 \pm 0.094$). It can be seen from these results that all values of the estimated myocardium model's parameters in our study are in a reasonable range. The differences among these results were mainly caused by the individual differences.

The SDs of the estimated parameters are relatively large in this study, especially for k_3 and k_4. This was mainly caused by the individual differences in the function of FDG metabolism and also caused a little by the estimation bias. Because the PET imaging has some limitations, such as low resolution, high noise lever, and partial volume effects, the obtained BTAC and TTAC from PET images are rather noisy and may have a certain deviation from the expected values. This results in a bias between the estimated parameters through curve fitting and the true values of the parameters. It can be seen from Table 1 that the AIC and SC in fitting the pancreas's data are relatively large when compared with the other tissues' values. This was mainly caused by the relatively small size of the pancreas identified in the PET images. Because the tissue activity values were calculated by averaging whole voxel's values within the ROI, the large ROI can effectively suppress the effects of statistical noise and make the obtained TAC smooth. The TAC derived from smaller ROI is noisier and increases the WRSS in the curve fitting. In this study, we drew the ROIs as largely as possible in the several plans of the 3D image data under the doctors' guidance. Actually, the ROIs drawn in our study were the "volume of interest (VOI)".

In this work, the arterial and portal vein BTACs were derived from the PET image avoiding continual blood sampling from human blood vessel. Therefore, the dual-input analysis is possible in clinical practice. It can be seen from Table 2 that the parameter estimation results using dual-input were significantly different from that using arterial-input. Better fittings were obtained using the dual-input function rather than the arterial-input function, as shown by the lower AIC and SC scores in the dual-input analysis. The use of the arterial-input function underestimated the values of k_1, k_2, and f. The estimated values of k_3, k_4, and K were almost unaffected by the use of arterial-input. Therefore, the dual-input analysis is necessary in the human liver kinetic studies of FDG metabolism.

The seven tissues' model parameters of FDG metabolic kinetics were estimated in this study. Together with published model parameters of gray matter, white matter, and skeletal muscle, a relatively complete whole-body model was presented. This model provides the functional information of FDG metabolism in human body. Using the FDG kinetic model, we can further investigate the glucose metabolism, such as the noninvasive determination of local metabolic rate of glucose. The mathematical modeling is also the basis of simulation of a physiological process. With mathematical calculation, the FDG distribution process in human body after injection can be simulated and visualized based on the metabolic model and anatomical structure[24]. Although the whole-body model presented in this study includes the tissues of stomach, spleen, pancreas, and marrow, which have been rarely investigated before, this model is lack of several other large parts including the intestine and excretory system. The intestine is not very clear in the PET image, so a more effective method is needed to obtain the TTAC. For the excretory system, the three-compartment and four-parameter model is not suitable anymore for describing its kinetics of FDG metabolism. An appropriate mathematical model is needed to describe the excretory process of FDG in human body according to the actual physiological mechanism of FDG metabolism.

4 Conclusion

In this study, the FDG distribution kinetics in the tissues of myocardium, lung, liver, stomach, spleen, pancreas, and marrow, were investigated using dynamic FDG-PET, and the kinetic parameters were estimated. The comparison of parameter estimations using dual-input and arterial-input showed that the dual-input analysis is necessary in the human liver kinetic studies of FDG metabolism.

Acknowledgement The authors would like to thank the staff of the Department of Nuclear Medicine, General Hospital of PLA, Beijing, China, for their kindly support in making this study possible.

References

1 Jastrow H. and Vollrath L. Teaching and learning gross anatomy using modern electronic media based on the visible human project. Clin. Anat., 2003, 16(1): 44—54.

2 Pommert A., Hohne K. H., Pflesser B. et al. Creating a high-resolution spatial/symbolic model of the inner organs based on the Visible Human. Med. Image Anal., 2001, 5(3): 221—228.

3 Hohne K. H., Pflesser B., Pommert A. et al. A realistic model of human structure from the visible human data. Methods Inf. Med., 2001, 40(2): 83—89.

4 Spitzer V. M. and Whitlock D. G. The visible human dataset: The anatomical platform for human simulation. Anat. Rec., 1998, 253(2): 49—57.

5 Feng D., Li X. and Huang S. C. A new double modeling approach for dynamic cardiac PET studies using noise and spillover contaminated LV measurements. IEEE Transactions on Biomedical Engineering, 1996, 43(3): 319—327.

6 Huang S. C., Phelps M. E., Hoffman E. J. et al. Noninvasive determination of local cerebral metabolic rate of glucose in man. American Journal of Physiology - Endocrinology and Metabolism, 1980, 238: 69—82.

7 Reinhardt M., Beu M., Vosberg H. et al. Quantification of glucose transport and phosphorylation in human skeletal muscle using FDG PET. Journal of Nuclear Medicine, 1999, 40(6): 977—985.

8 Wong K. P., Feng D., Meikle S. R. et al. Simultaneous estimation of physiological parameters and the input function-in vivo PET data. IEEE Transactions on Information Technology in Biomedicine, 2001, 5(1): 67—76.

9 Selberg O., Muller M. J., van den Hoff J. et al. Use of positron emission tomography for the assessment of skeletal muscle glucose metabolism. Nutrition, 2002, 18(4): 323—328.

10 Richard M. L. and Qi J. Statistical approaches in quantitative positron emission tomography. Statistics and Computing, 2000, 10: 147—165.

11 Hays M. T. and Segall G. M. A mathematical model for the distribution of fluorodeoxyglucose in humans. Journal of Nuclear Medicine, 1999, 40(8): 1358—1366.

12 Munk O. L., Bass L., Roelsgaard K. et al. Liver kinetics of glucose analogs measured in pigs by PET: Importance of dual-input blood sampling. Journal of Nuclear Medicine, 2001, 42(5): 795—801.

13 Chen S. and Feng D. Noninvasive quantification of the differential portal and arterial contribution to the liver blood supply from PET measurements using the ^{11}C-acetate kinetic model. IEEE Transactions on Biomedical Engineering, 2004, 51(9): 1579—1585.

14 Correia J. A bloody future for clinical PET. Journal of Nuclear Medicine, 1992, 33: 620—622.

15 Takikawa S., Dhawan V., Spetsieris P. et al. Noninvasive quantitative fluorodeoxyglucose PET studies with an estimated input function derived from a population-based arterial blood curve. Radiology, 1993, 188(1): 131—136.

16 Chen K., Bandy D., Reiman E. et al. Noninvasive quantification of the cerebral metabolic rate for glucose using positron emission tomography, F-18-fluoro-2-deoxyglucose, the Patlak method, and an image-derived input function. J. Cereb. Blood Flow Metab., 1998, 18(7): 716—723.

17 van der Weerdt A. P., Klein L. J., Boellaard R. et al. Image-derived input functions for determination of MRGlu in cardiac F-18-FDG PET scans. Journal of Nuclear Medicine, 2001, 42(11): 1622—1629.

18 Chen S., Ho C., Feng D. et al. Tracer kinetic modeling of ^{11}C-acetate applied in the liver with positron emission tomography. IEEE Transactions on Medical Imaging, 2004, 23(4): 426—432.

19 Akaike H. A new look at the statistical model identification. IEEE Trans. Automac. Contr., 1974, AC-19: 716—723.

20 Schwarz G. Estimating the dimension of a model. Ann. Statist., 1978, 6: 461—564.

21 Bertoldo A., Vicini P., Sambuceti G. et al. Evaluation of compartmental and spectral analysis models of [^{18}F] FDG kinetics for heart and brain studies with PET. IEEE Transactions on Biomedical Engineering, 1998, 45(12): 1429—1448.

22 Li X., Feng D., Lin K. P. et al. Estimation of myocardial glucose utilization with PET using the left ventricular time-activity curve as a non-invasive input function. Medical & Biological Engineering & Computing, 1998, 36(1): 112—117.

23 Li X., Feng D. and Chen K. Optimal image sampling schedule for both image-derived input and output functions in PET cardiac studies. IEEE Transactions on Medical Imaging, 2000, 19(3): 233—242.

24 Cui Y. and Bai J. Method of simulation and visualization of FDG metabolism based on VHP image. In: Medical Imaging 2005: Visualization, Image-Guided Procedures, and Display, vol. 5744, Proceedings of the Society of Photo-Optical Instrumentation Engineers (SPIE). San Diego, CA, United States, Feb 13—15, 2005, 547—554.